REPORT

Selectivity switch via tuning surface static electric field in photocatalytic alcohol conversion

Zhiwei Chen,[1] Hongru Zhou,[1] Fanhao Kong,[1] Zhaolin Dou,[1] and Min Wang[1,*]
*Correspondence: wangmin@dlut.edu.cn

Received: March 10, 2024; Accepted: June 16, 2024; Published Online: June 17, 2024; https://doi.org/10.1016/j.xinn.2024.100659

www.the-innovation.org

GRAPHICAL ABSTRACT

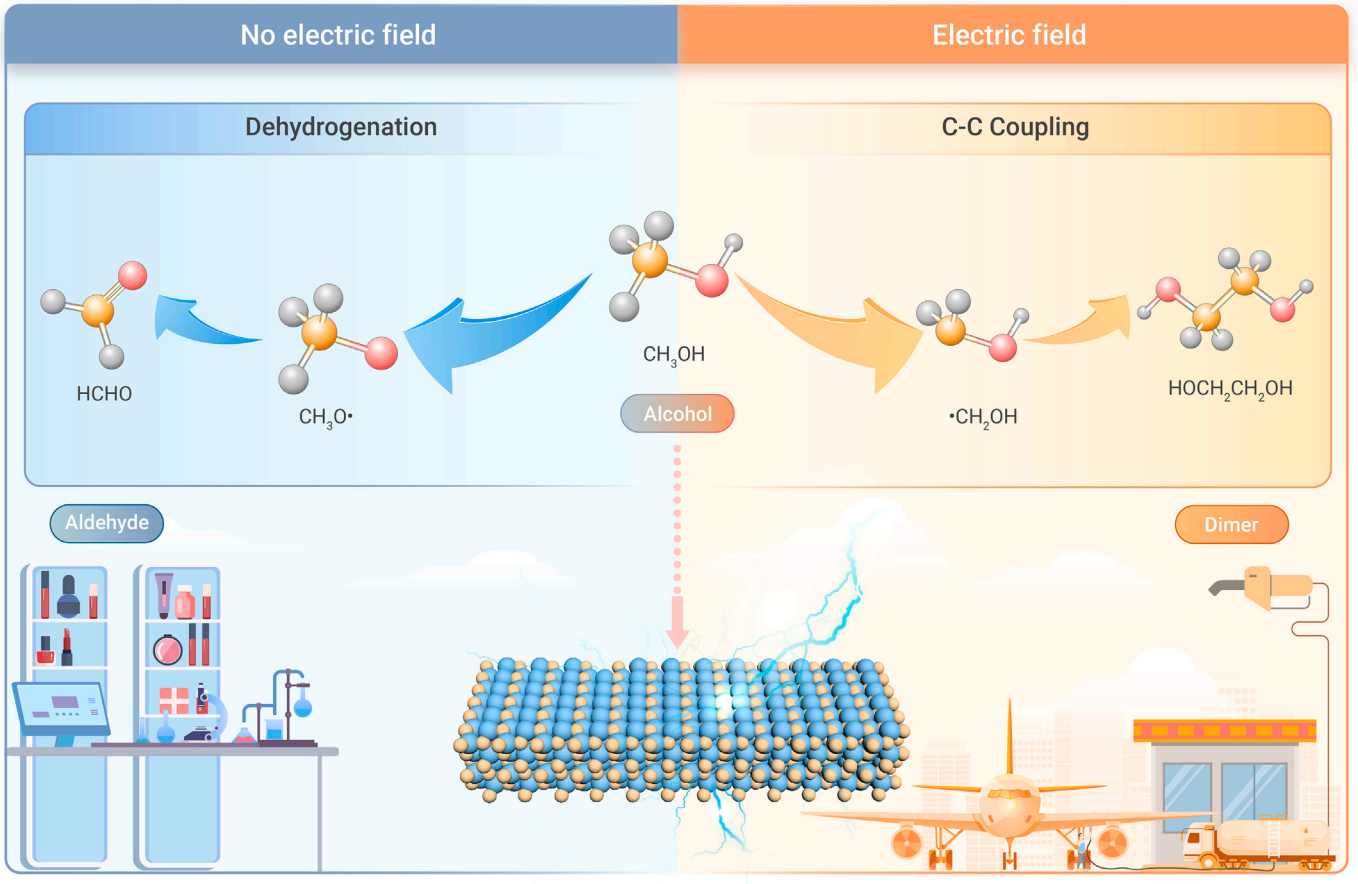

PUBLIC SUMMARY

- Selectivity control in the photocatalytic conversion of alcohols via engineering the surface static electric field of the CdS semiconductor has been achieved.
- The intensity of the surface static electric field can be controlled via Au–CdS interaction induced lattice strain.
- The induced surface static electric field preferentially activates the C–H bond over the O–H bond and changes the selectivity from aldehydes to dimers.

REPORT

Selectivity switch via tuning surface static electric field in photocatalytic alcohol conversion

Zhiwei Chen,[1] Hongru Zhou,[1] Fanhao Kong,[1] Zhaolin Dou,[1] and Min Wang[1,*]

[1]State Key Laboratory of Fine Chemicals, School of Chemistry, Dalian University of Technology, Dalian 116024, China

*Correspondence: wangmin@dlut.edu.cn

Received: March 10, 2024; Accepted: June 16, 2024; Published Online: June 17, 2024; https://doi.org/10.1016/j.xinn.2024.100659

Citation: Chen Z., Zhou H., Kong F., et al., (2024). Selectivity switch via tuning surface static electric field in photocatalytic alcohol conversion. The Innovation **5(5)**, 100659.

Photocatalysis has shown great potential in organic reactions, while controlling the selectivity is a long-standing goal and challenge due to the involvement of various radical intermediates. In this study, we have realized selectivity control in the photocatalytic conversion of alcohols via engineering the surface static electric field of the CdS semiconductor. By leveraging the Au–CdS interaction to adjust lattice strain, which influences the intensity of the surface static electric field, we altered the pathways of alcohol conversion. The increased intensity of the surface static electric field changed the activation pathways of the C–H/O–H bond, leading to the selective formation of targeted C/O-based radical intermediates and altering the selectivity from aldehydes to dimers. A wide range of alcohols, such as aromatic alcohol and thiophenol alcohol, were selectively converted into aldehyde or dimer. This work provides an effective strategy for selectively controlling reaction pathways by generating a surface electric field.

INTRODUCTION

Photocatalysis shows great potential in a series of chemical reactions due to its utilization of renewable solar energy and operation under mild conditions.[1–10] However, controlling the selectivity of chemical reactions, particularly in semiconductor-based photocatalytic organic reactions involving hydrogen abstraction from the O/C–H bond to form various radicals, remains a long-standing challenge.[11–19] As exemplified by photocatalytic alcohol conversion, C–H bond cleavage will generate carbon-centered radicals and produce dimers via C–C bond coupling, while O–H bond cleavage usually favors aldehyde formation.[20–22] Methanol is a plentiful and renewable C1 feedstock derived from both fossil resources and biomass resources.[23,24] The dehydrogenation of methanol will produce formaldehyde, which is the major component in fixatives and disinfectors,[25,26] while the dehydrocoupling of methanol will generate ethylene glycol (EG), which is a widely used diol for the synthesis of polyethylene terephthalate.[27] The selective upgrading of methanol to either formaldehyde or EG is highly attractive but very challenging due to involving various reactive intermediates.[28] Overall, present studies show selectivity to either formaldehyde or EG, but lack an efficient method to control the selectivity.[29–31]

The electric field can change the activation barriers by interacting with the dipoles of chemical bonds and thus affecting the reactivity and selectivity.[32–34] Most works use an external electric field for organic reactions, such as the Diels-Alder (D-A) reaction and aldehyde ammoxidation, which generally needs extra voltage or salt additives.[35–39] The intrinsic electric field occurs naturally in semiconductors.[40,41] The surface of the semiconductor is usually charged by accepting/donating electrons from/to the bulk to match the Fermi level due to the structural differences between the bulk phase and surface state.[42,43] Once the as-indued surface electric field is strong enough to alter the energies of molecular orbitals of adsorbates, it is expected to affect the activation of adsorbates and tune the selectivity, but this has been rarely explored.[44,45]

The charges on the surface are heavily affected by electron transfer between the surface state and bulk phase. The greater structural differences between the bulk phase and surface state will accumulate more charges on the surface.[46] Consequently, the strength of the surface electric field could be enhanced via tuning the surface structure to induce more structural differences to bulk phase. Herein, we intend to reveal the effect of the surface static electric field (SSEF) of CdS on photocatalytic alcohol conversion. We use metal-support interaction to distort the surface structure over Au/CdS. The strong interaction between Au and CdS creates lattice strain, contributing to the formation of the SSEF. The intensity of the SSEF is tunable via adjusting the lattice strain. The introduction of the SSEF changes the pathways of alcohol conversion by differential activation of the C–H/O–H bond of alcohol adsorbates, resulting in changing the selectivity from aldehydes to dimers. This work provides new inspiration to utilize surface electric field to control selectivity for photocatalysis.

RESULTS

Theoretical calculation of the electric field effect

The conversion of methanol usually involves the activation of its O–H or C–H bond, resulting in the formation of different C/O-based radical intermediates (Figure 1A).[47,48] The electric field could activate the chemical bonds via affecting their dipoles.[49] Considering that the O–H and C–H bonds show differential polarity,[50] it is possible to selectively activate the O–H/C–H bond via introducing the electric field. To explore this, we conducted density functional theory (DFT) calculations to investigate the effect of the electric field on the O–H/C–H bond cleavage of methanol. The electric field shows a stronger effect on the polar O–H bond compared to the C–H bond. The change of C–H bond length was negligible with increasing the electric field, while the O–H bond length was shortened by 1.2%, rendering the O–H bond more difficult to break (Figure 1B). Moreover, as the electric field increased, the formation energy (ΔE) of $\cdot OCH_3$ radicals increases to 2.4 eV, while the ΔE of $\cdot CH_2OH$ radicals decreases to 1.9 eV, indicating that preferential cleavage of the C–H bond occurs over the O–H bond in the presence of the electric field (Figure 1C). Calculation results demonstrate that the electric field favors C–H bond cleavage and prohibits O–H bond cleavage. Therefore, the differential activating C–H/O–H bond by the electric field is supposed to effectively tune the reaction pathways of alcohol conversion.

The strain analysis of Au/CdS

Then, we try to introduce the electric field in the photocatalytic system. Different from previous works that use an external electric field, we intend to utilize the SSEF of semiconductors, which naturally exists but is usually too weak to affect the reaction. The challenge is to control the intensity of the SSEF on CdS. The charges on the surface will generate the SSEF, and tuning the surface charges is an effective way to control the SSEF. The surface charges rely heavily on the electron transfer between the surface state and bulk phase. The greater structural differences between the bulk phase and surface state will lead to more charges accumulating on the surface.[43] Then, we tried to increase the strength of the SSEF via tuning the surface structure of CdS to induce more structural differences to the bulk phase. This was achieved through metal-support interaction, which distorts the surface structure and is reflexed by lattice strain. Au/CdS with tunable lattice strain was prepared via an acidity regulation strategy. The strain intensity was positively correlated to the acidity and thus can be easily regulated.

Au/CdS samples were prepared via impregnation of gold in the aqueous solution with different pH values, denoted as AC-x, x = 1, 2, 3, and 4, corresponding to the pH values of 4.1, 2.8, 1.7, and 0.5, respectively (Figure 2A). The Au content of all samples was nearly 1.9 wt % as determined by inductively coupled plasma-optical emission spectroscopy (ICP-OES) (Table S1). X-ray diffraction patterns revealed that all the Au/CdS samples exhibited typical hexagonal CdS with a space group of P63mc (JCPDS no. 41-1049) (Figure 2B).[51] The increase of acidity induces stronger metal-support interaction and makes the lattice compressed, as evidenced by the shift of the CdS (102) plane toward the higher angle. The lattice parameters decrease from a = b = 4.1486 and c = 6.7464 Å to a = b = 4.1192 and c = 6.6920 Å (Figure S1). The effect of acidity on Au–CdS interaction

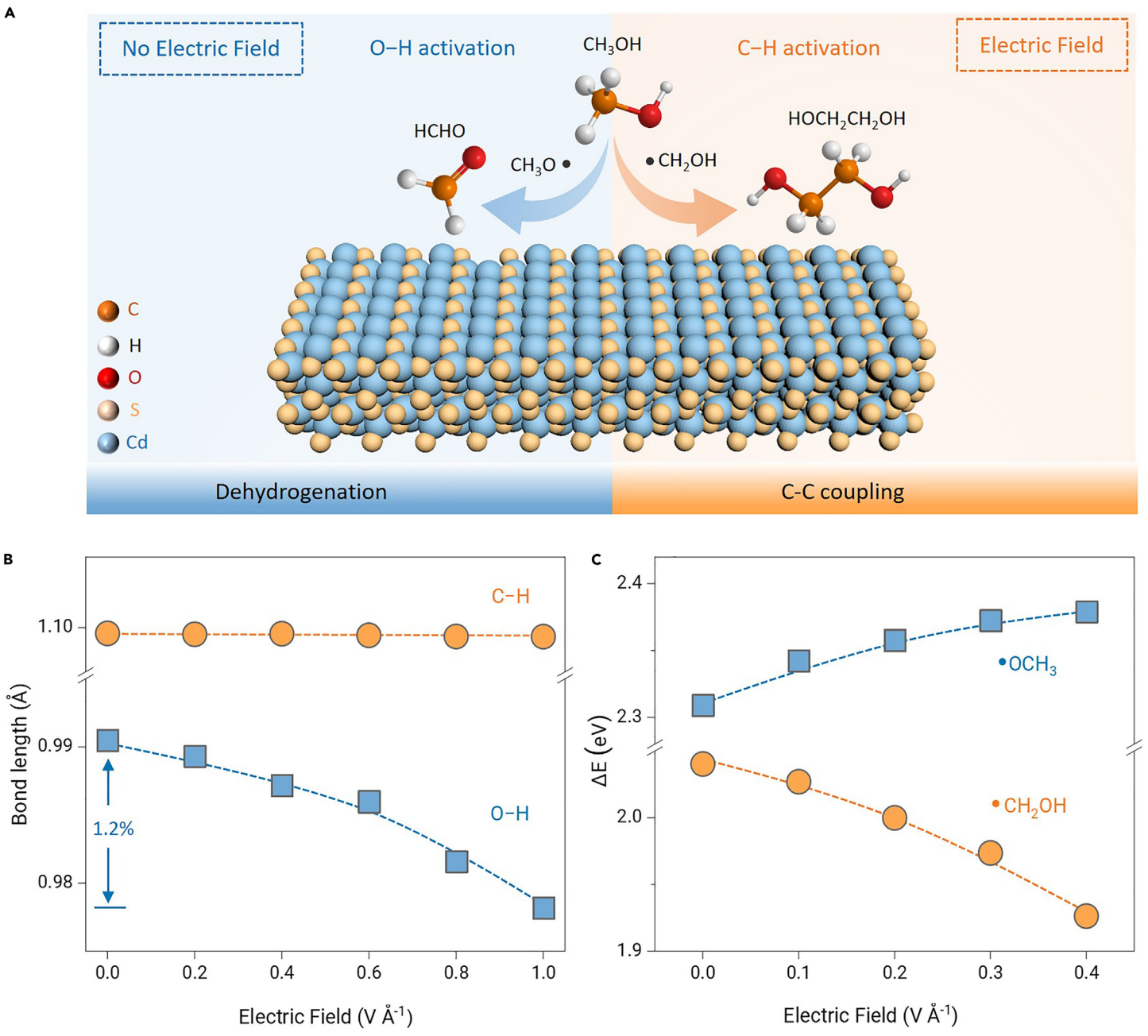

Figure 1. The concept of electric field tuning the reaction pathways of methanol conversion on CdS (A) Scheme of the electric field tuning the pathways of methanol conversion on CdS (100) facet. (B) The change of C–H/O–H bond length with increasing the electric field. (C) The formation energy of $\cdot OCH_3$ and $\cdot CH_2OH$ radicals on CdS (100) facet with increasing the electric field.

was further confirmed by X-ray photoelectron spectroscopy characterization. The peaks of Au 4f shift toward lower binding energy by 0.1 eV accompanied by the positive shift of S 2p peak, indicating the strong interaction between Au and CdS, and the photoinduced electrons could effectively transfer from CdS to Au (Figures S2–S4).[52–54] The lattice strain can be controlled via tuning the acidity, as shown by the positive increase of lattice strain with the acidity (Figure 2C). All Au/CdS samples show similar light adsorption and band gap, and no obvious surface plasmon resonance effect was observed (Figure S5).

The effect of Au–CdS interaction on lattice strain was further investigated by transmission electron microscope characterization. Au nanoparticles with the size of 3.2–4.1 nm were dispersed on a CdS nanorod (Figures S6 and S7). AC-1 shows weak Au–CdS interaction, as evidenced by a large contact angle of 134° (Figure 2D), while the interaction is stronger in AC-4 with a contact angle of 75° (Figure 2E).[55] The stronger Au–CdS interaction shrinks the CdS (102) plane lattice from 2.504 to 2.467 Å (Figure S8). As shown in geometric phase analysis, the more obvious color contrast of AC-4 further reveals a larger lattice strain in AC-4 than in AC-1 (Figure S9).[56] The above results confirmed that the Au–CdS interaction becomes stronger with the increase of the acidity and, consequently, causes lattice contraction.

The analysis of electric field

Lattice strain usually leads to nonuniform charge distribution on the surface and bulk of semiconductors due to breaking of the symmetry of crystal structures, thus contributing to the formation of the internal electric field (IEF).[57] DFT calculations were performed to investigate the effect of charge distributions induced by lattice strain over Au/CdS. Au slightly contacting with CdS exhibits a 0.7 eV electric potential (V_{BB}) difference between the surface and bulk, whereas stronger Au–CdS interaction leads to a larger V_{BB} difference (2.6 eV) (Figure S10). The structural differences between the surface layer and bulk phase lead to nonuniform charge distribution on the surface and bulk of CdS (Figure 3A), forming the IEF in the space region (blue area).[57] The relative IEF intensity of Au/CdS samples, measured based on the model proposed by Kanata et al. (Figures S11 and S12),[58] was increased with the increase of lattice strain (Figure S13). Consequently, the increased IEF effectively facilitates the charge separation and inhibits

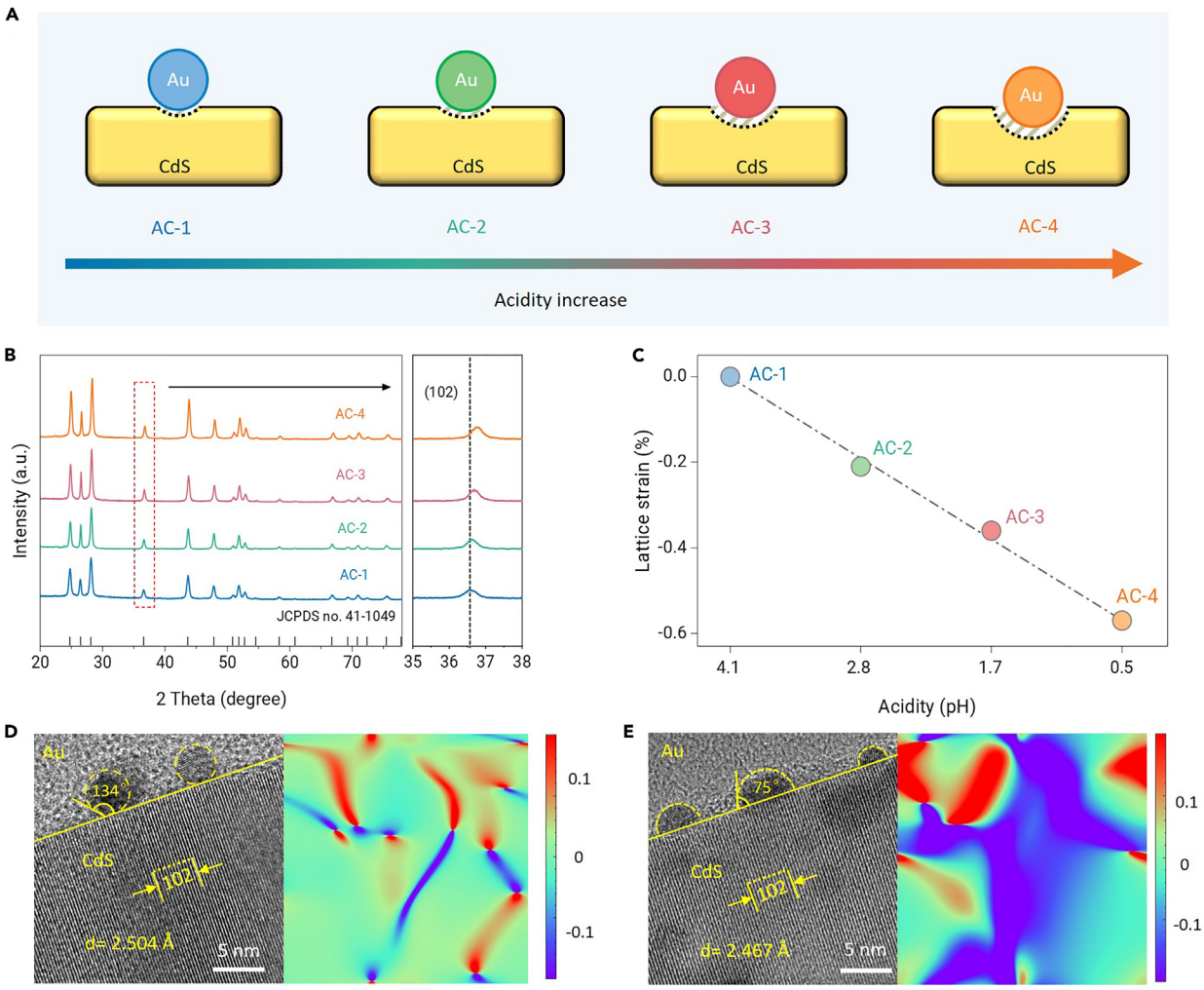

Figure 2. The strain analysis of Au/CdS (A) Scheme of the preparation of Au/CdS samples with the acidity regulation. (B) X-ray diffraction patterns of Au/CdS samples. (C) The relationship between lattice strain of Au/CdS samples and acidity. (D and E) High-resolution transmission electron microscopy images and ε_{xx} strain component determined via geometric phase analysis of AC-1 and AC-4 samples.

their recombination, as evidenced by the stronger photocurrent response, smaller Nyquist plots, weaker fluorescence intensity, and longer carrier lifetime (Figures S14–S17).[59]

The charges accumulating on the surface generate a SSEF (gray area). The magnitude of the SSEF can be determined through the carrier concentration (Figure S18) and the depletion layer thickness (*D*) (for detailed calculations, see the supplemental information).[60–62] The *D* could be reflected by the V_{BB}. The V_{BB} at the surface of samples was measured by surface photovoltage.[63] With the increase of lattice strain, the V_{BB} increases from 54 to 217 mV (Figure 3B), and the *D* increases from 5.93 to 8.40 nm. More compressive lattice strain leads to greater structural differences between the bulk phase and surface layer, leading to a wider depletion layer. Consequently, more electrons accumulate on the surface layer and thus generate a larger V_{BB}. The intensity of the SSEF in the AC−4 sample is 3.1 times that of the AC-1 sample (Figure 3C). The above results illustrated that the larger lattice strain will induce a stronger SSEF.

SSEF regulated methanol conversion

To evaluate the effect of the SSEF on the reaction, photocatalytic methanol conversion was performed in a homemade quartz tube reactor (6.5 mL) and irradiated by a 455 nm light-emitting diode. There are two pathways for methanol conversion. One is the dehydrogenation to HCHO, and the other is C−C bond coupling to EG (Figure 4A). H_2, HCHO, and EG were almost linearly produced as the reaction proceeded (Figures 4B–4D and S19). Compared with the AC-1 catalyst, the productivities of HCHO and EG of other samples were both increased and released more H_2, which could be attributed to effective charge separation (Figure 4E). More importantly, the SSEF changes the reaction pathways. The dehydrogenation reaction is prohibited, and the C−C bond coupling reaction is promoted, via increasing the intensity of the SSEF, which was consistent with DFT calculation results that the electric field favors C−H bond cleavage and prohibits O−H bond cleavage. For AC-1 with a weak SSEF, the O−H bond cleavage is favored to form HCHO forms, while for AC-4 with a stronger SSEF, C−H bond cleavage is more favored to produce EG. Consequently, the selectivity is changed from 100% of HCHO to 92% of EG (Figure 4F). Compared with previous works, the selectivity of HCHO or EG is excellent (Table S2). When the reaction was conducted in acetonitrile solvent, AC-1 shows 45% conversion of the methanol with 88% carbon yield of HCHO (carbon balance: 88%). AC-4 shows 99% conversion of methanol with 82% carbon yield of EG, 8% carbon yield of HCHO, and 1% carbon yield of glycoaldehyde (carbon balance: 91%) (Figure S20).

Besides methanol, we have performed photocatalytic conversion of other alcohols, including aromatic alcohol and thiophenol alcohol, using the AC-1 and AC-4 catalysts (Table 1). AC-1 with a weak SSEF is selective to produce the corresponding aldehydes with 60%–98% yield and 94%–99% conversion. On the other hand, AC-4 with a strong SSEF prefers to form coupling products with 63%–83% yield and 95%–99% conversion. These results demonstrate the feasibility of the SSEF in tuning the selectivity in photocatalytic alcohol conversion.

Reaction mechanism

We performed deep studies to elucidate the reaction mechanism of methanol conversion under the effect of the SSEF. The addition of styrene nearly completely suppressed the formation of HCHO and EG, suggesting a radical route mechanism (Figure S21). The $\cdot CH_2OH$ radical adducts were detected by gas chromatography-mass spectrometry (Figure S22). *In situ* electron spin resonance spectra (Figure 5A) using 5,5-dimethyl-1-pyrroline-N-oxide as a spin-trapping agent reveals the generation of the $\cdot CH_2OH$ and $\cdot OCH_3$ radicals

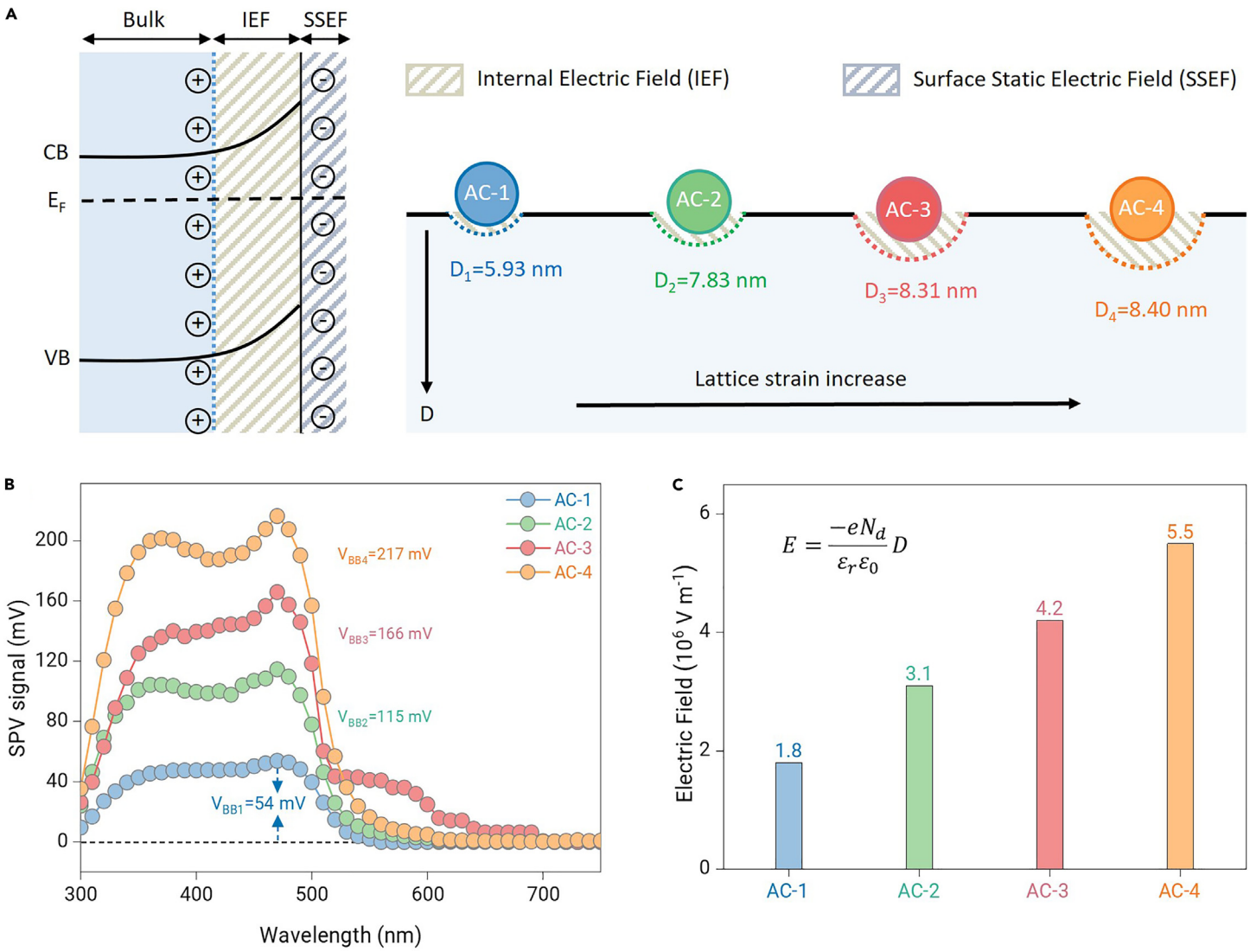

Figure 3. The analysis of the electric field (A) Scheme of the electric field distribution and the thickness of depletion layer of Au/CdS samples with lattice strain increasing. (B) Surface photovoltage (SPV) signals of Au/CdS samples. (C) The intensity of SSEF of Au/CdS samples. In the equation, E is the intensity of the surface static electric field, e is the elementary charge, D is the depletion layer thickness, N_d is the carrier concentration, ε_r is the relative constant, and ε_0 is the permittivity of vacuum.

(Figure 5B).[30] The $\cdot CH_2OH$ radical derived from C–H bond cleavage accounts for the EG formation, whereas the $\cdot OCH_3$ radical resulting from O–H bond cleavage is responsible for HCHO formation. DFT calculation results have revealed that increasing the electric field will favor the formation of CH_2OH radicals and prohibit the formation of $\cdot OCH_3$ radicals (Figure 1C). This will lead to the generation of different ratios of C/O-centered radicals, which is demonstrated by the following radical trapping experiment. The $\cdot OCH_3$ radicals are dominant (80%) in AC-1 with a weak SSEF, while AC-4 with a stronger SSEF exhibited a higher percentage of $\cdot CH_2OH$ radicals (65%), indicating that the SSEF is more inclined to selectively activate the C–H bond than the O–H bond, thus changing the reaction pathway.

Methanol adsorption Fourier transform infrared (FTIR) spectroscopy was carried out to further investigate the C–H/O–H bond activation mechanism (Figure S23). After the introduction of methanol vapor, the C–H stretching vibration peak (2,948 cm^{-1} over AC-1) exhibited a negligible change (2,945 cm^{-1} over AC-4).[64] By contrast, the O–H stretching vibration peak was blue-shifted from 3,347 to 3,496 cm^{-1} after methanol adsorption on AC-4, indicating that the O–H bond length shortened and was difficult to activate, consistent with the previous DFT calculations about the change of C–H/O–H bond length (Figure 1B). The above results revealed that AC-4 has difficulty activating the O–H bond, thus prohibiting the formation of aldehyde.

Attenuated total reflection FTIR spectroscopy was employed to investigate the photocatalytic conversion of methanol (Figure 5C). As the light irradiation time prolonged, a new peak at 1,728 cm^{-1} assigned to the carbonyl group of HCHO appeared and gradually increased for both AC-1 and AC-4 samples.[65] Besides, an additional band centered at 1,460 cm^{-1} assigned to C–C bond symmetric stretching of EG was observed in AC-4 samples but not in AC-1 samples.[66] The introduction of the electric field makes the scission of the O–H bond difficult to generate $\cdot OCH_3$ radicals, and preferentially activates the C–H bond for the formation of $\cdot CH_2OH$ radicals, thus tuning the products selectivity.

The density of states shows that the valence band of Au/CdS is mainly composed of S orbitals and the conduction band primarily originates from the Au orbitals, indicating that the holes accumulate on S and electrons accumulate on Au (Figure S24). Herein, we proposed a possible photocatalytic reaction mechanism (Figure 5D). Photoirradiation of Au/CdS generates holes and electrons. For AC-1 with a weak SSEF, the holes on CdS attack the O–H bond of methanol and afford $\cdot OCH_3$ radicals, which are further converted into HCHO. By contrast, for AC-4 with a strong SSEF, the holes on CdS prefer to activate the C–H bond and produce $\cdot CH_2OH$ radicals that subsequently couple to EG. The photoinduced electrons transfer to Au and reduce the protons to generate H_2.

CONCLUSION

In summary, we demonstrated that the SSEF can alter the reaction pathways in the photocatalytic alcohol conversion over Au/CdS. The intensity of the SSEF can be adjusted via Au–CdS-interaction-induced lattice strain. The induced SSEF preferentially activates the C–H bond over the O–H bond and changes the selectivity from aldehydes to dimers. Through this strategy, we realized the selective formation of aldehydes or dimers from photocatalytic conversion of alcohols via

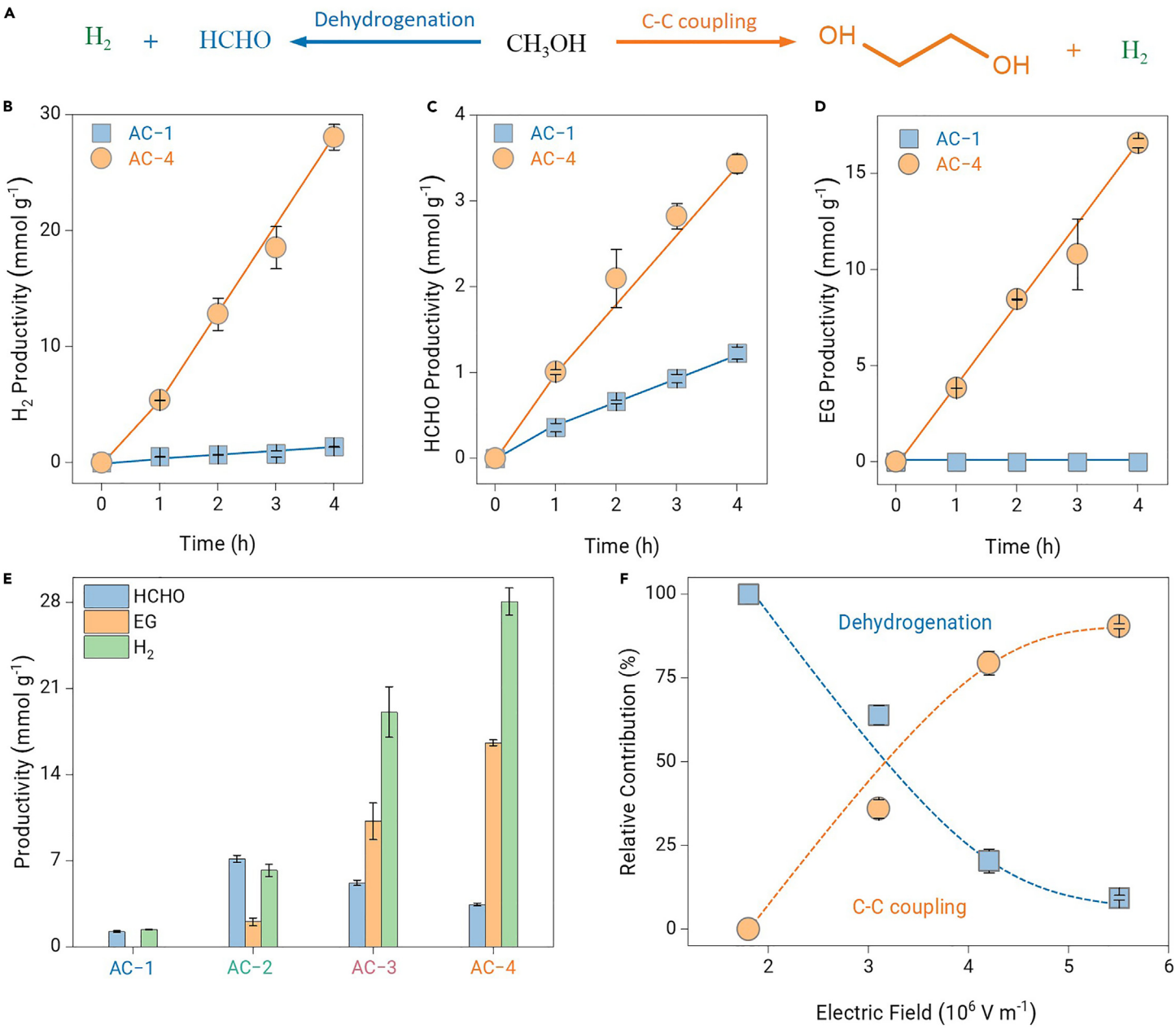

Figure 4. SSEF regulated methanol conversion (A) Two pathways of photocatalytic methanol conversion. (B–D) The time profiles of H_2, HCHO, and EG productivity over AC-1 and AC-4 samples. (E) The performance of photocatalytic methanol conversion over Au/CdS samples. (F) The product selectivity under different SSEFs. Reaction conditions: 5 mg of catalyst, 1 mL of methanol, 1 atm of Ar, 455 nm LED. The error bars represent the relative deviation derived from parallel experiments.

tuning the SSEF. This study provides a new idea for designing tailored catalysts to steer the reaction pathway in semiconductor-based photocatalysis via utilizing the surface electric field. In this strategy, the electric field can differentially affect the chemical bond with different polarity, which is promising to be applicable for selectivity control in organic synthesis involving polar molecules. Further works will be devoted to the develop new method to effectively tune the SSEF for various semiconductors beyond CdS.

MATERIALS AND METHODS

See the supplemental information for details.

REFERENCES

1. Dhull, P., Sudhaik, A., Raizada, P., et al. (2023). An overview on ZnO-based sonophotocatalytic mitigation of aqueous phase pollutants. Chemosphere ***333***: 138873. https://doi.org/10.1016/j.chemosphere.2023.138873.
2. Kumar, A., Singh, P., Nguyen, V.-H., et al. (2023). Rationally constructed synergy between dual-vacancies and Z-scheme heterostructured MoS_{2-x}/g-C_3N_4/Ca-α-Fe_2O_3 for high-performance photodegradation of sulfamethoxazole antibiotic from aqueous solution. Chem. Eng. J. ***474***: 145720. https://doi.org/10.1016/j.cej.2023.145720.
3. Dhull, P., Sudhaik, A., Sharma, V., et al. (2023). An overview on $InVO_4$-based photocatalysts: Electronic properties, synthesis, enhancement strategies, and photocatalytic applications. Mol. Catal. ***539***: 113013. https://doi.org/10.1016/j.mcat.2023.113013.
4. Sharma, K., Kumar, A., Ahamad, T., et al. (2023). Sulphur vacancy defects engineered metal sulfides for amended photo(electro)catalytic water splitting: A review. J. Mater Sci. Tech. ***152***: 50–64. https://doi.org/10.1016/j.jmst.2022.11.053.
5. Dutta, V., Sonu, S., Raizada, P., et al. (2023). Prism-like integrated Bi_2WO_6 with Ag-$CuBi_2O_4$ on carbon nanotubes (CNTs) as an efficient and robust S-scheme interfacial charge transfer photocatalyst for the removal of organic pollutants from wastewater. Environ. Sci. Pollut. Res. Int. ***30***(60): 124530–124545. https://doi.org/10.1007/s11356-022-20743-8.
6. Sharma, K., Hasija, V., Malhotra, M., et al. (2024). A review of CdS-based S-scheme for photocatalytic water splitting: Synthetic strategy and identification techniques. Int. J. Hydrogen Energy ***52***: 804–818. https://doi.org/10.1016/j.ijhydene.2023.09.033.
7. Chen, Z., Zhou, H., Kong, F., et al. (2024). Photocatalytic Conversion of Lipid to Diesel and Syngas via Engineering the Surface Proton Transfer. ACS Catal. ***14***(3): 1699–1705. https://doi.org/10.1021/acscatal.3c04818.
8. Chen, J.M. (2021). Carbon neutrality: Toward a sustainable future. Innovation ***2***(3): 100127. https://doi.org/10.1016/j.xinn.2021.100127.

Table 1. Substrate scope of photocatalytic alcohol conversion

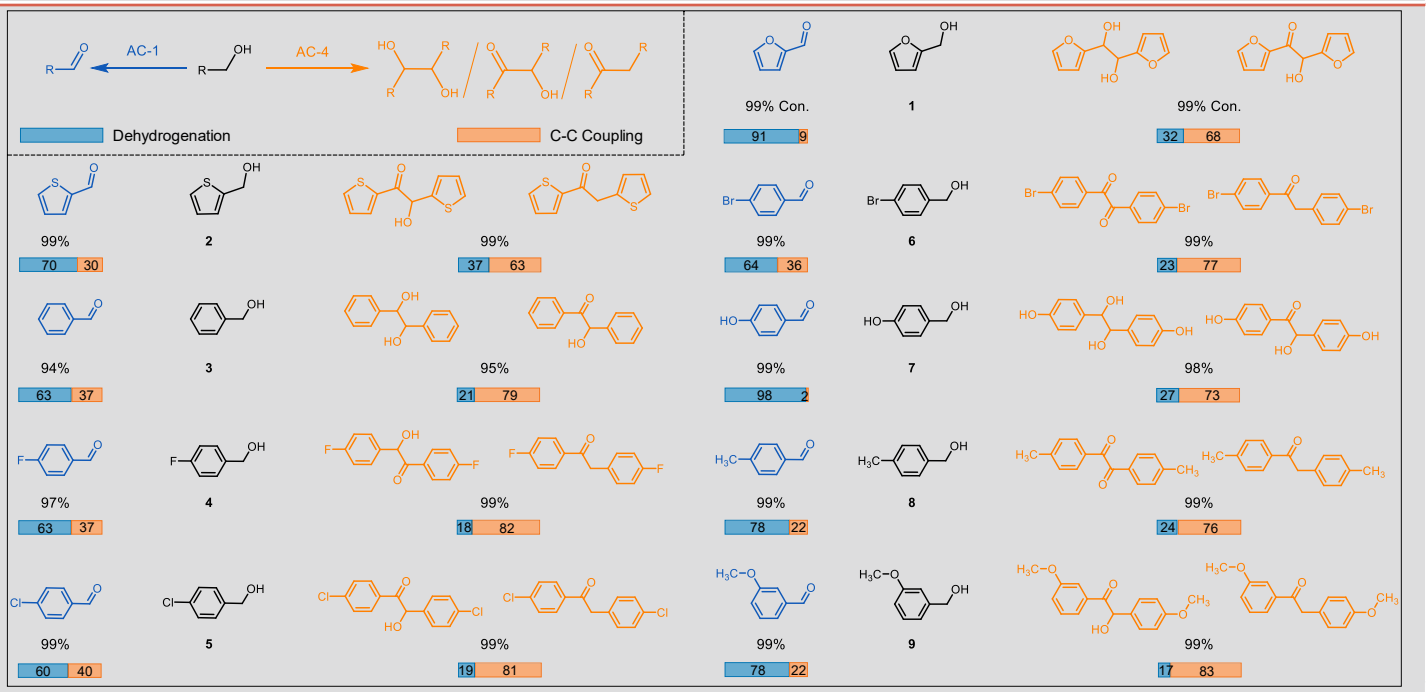

Reaction conditions: 5 mg of catalysts, 5 mg of substrate, 1 mL of CH_3CN, 1 atm of Ar, 455 nm LED, 6 h.

9. Queneau, Y., and Han, B. (2022). Biomass: Renewable carbon resource for chemical and energy industry. Innovation ***3***(1): 100184. https://doi.org/10.1016/j.xinn.2021.100184.
10. Shuai, L., and Song, B. (2024). Biomass valorization assisted by protection strategies. The Innovation Materials ***2***(1): 100046. https://doi.org/10.59717/j.xinn-mater.2024.100046.
11. Yu, X.Y., Chen, J.R., and Xiao, W.J. (2021). Visible Light-Driven Radical-Mediated C-C Bond Cleavage/Functionalization in Organic Synthesis. Chem. Rev. ***121***(1): 506–561.
12. Morcillo, S.P. (2019). Radical-Promoted C-C Bond Cleavage: A Deconstructive Approach for Selective Functionalization. Angew. Chem. Int. Ed. ***58***(40): 14044–14054. https://doi.org/10.1002/anie.201905218.
13. Qi, M.Y., Conte, M., Anpo, M., et al. (2021). Cooperative Coupling of Oxidative Organic Synthesis and Hydrogen Production over Semiconductor-Based Photocatalysts. Chem. Rev. ***121***(21): 13051–13085. https://doi.org/10.1021/acs.chemrev.1c00197.
14. Wang, M., Zhou, H., and Wang, F. (2023). Photocatalytic Production of Syngas from Biomass. Acc. Chem. Res. ***56***: 1057–1069. https://doi.org/10.1021/acs.accounts.3c00039.
15. Lee, K., Jing, Y., Wang, Y., et al. (2022). A unified view on catalytic conversion of biomass and waste plastics. Nat. Rev. Chem ***6***(9): 635–652. https://doi.org/10.1038/s41570-022-00411-8.
16. Li, Y.X., Xuan, Q.Q., Liu, L., et al. (2013). A Pd(0)-catalyzed direct dehydrative coupling of terminal alkynes with allylic alcohols to access 1,4-enynes. J. Am. Chem. Soc. ***135***(34): 12536–12539. https://doi.org/10.1021/ja406025p.
17. Wakerley, D.W., Kuehnel, M.F., Orchard, K.L., et al. (2017). Solar-driven reforming of lignocellulose to H_2 with a CdS/CdO_x photocatalyst. Nat. Energy ***2***(4): 17021. https://doi.org/10.1038/nenergy.2017.21.
18. Li, S., Dong, M., Peng, M., et al. (2022). Crystal-phase engineering of PdCu nanoalloys facilitates selective hydrodeoxygenation at room temperature. Innovation ***3***(1): 100189. https://doi.org/10.1016/j.xinn.2021.100189.
19. Zhao, B., Tan, H., Yang, J., et al. (2024). Catalytic conversion of mixed polyolefins under mild atmospheric pressure. Innovation ***5***(2): 100586. https://doi.org/10.1016/j.xinn.2024.100586.
20. Wu, X., Li, J., Xie, S., et al. (2020). Selectivity Control in Photocatalytic Valorization of Biomass-Derived Platform Compounds by Surface Engineering of Titanium Oxide. Chem ***6***(11): 3038–3053. https://doi.org/10.1016/j.chempr.2020.08.014.
21. Zhang, S.Y., Zhang, F.M., and Tu, Y.Q. (2011). Direct Sp3α-C-H activation and functionalization of alcohol and ether. Chem. Soc. Rev. ***40***(4): 1937–1949. https://doi.org/10.1039/c0cs00063a.
22. Cheng, J.K., and Loh, T.P. (2015). Copper- and cobalt-catalyzed direct coupling of sp(3) alpha-carbon of alcohols with alkenes and hydroperoxides. J. Am. Chem. Soc. ***137***(1): 42–45. https://doi.org/10.1021/ja510635k.
23. Shih, C.F., Zhang, T., Li, J., et al. (2018). Powering the Future with Liquid Sunshine. Joule ***2***(10): 1925–1949. https://doi.org/10.1016/j.joule.2018.08.016.
24. Olah, G.A. (2013). Towards Oil Independence Through Renewable Methanol Chemistry. Angew. Chem. Int. Ed. ***52***(1): 104–107. https://doi.org/10.1002/anie.201204995.
25. Konno, K., Yamasaki, M., Miyazaki, T., et al. (2023). Glyoxal fixation: An approach to solve immunohistochemical problem in neuroscience research. Sci. Adv. ***9***(28): eadf7084. https://doi.org/10.1126/sciadv.adf7084.
26. Świetlik, J., Raczyk-Stanisławiak, U., and Nawrocki, J. (2009). The influence of disinfection on aquatic biodegradable organic carbon formation. Water Res. ***43***(2): 463–473. https://doi.org/10.1016/j.watres.2008.10.021.
27. Jiao, X., Zheng, K., Hu, Z., et al. (2021). Conversion of Waste Plastics into Value-Added Carbonaceous Fuels under Mild Conditions. Adv. Mater. ***33***(50): 2005192. https://doi.org/10.1002/adma.202005192.
28. Moran, J., Preetz, A., Mesch, R.A., et al. (2011). Iridium-catalysed direct C–C coupling of methanol and allenes. Nat. Chem. ***3***(4): 287–290. https://doi.org/10.1038/nchem.1001.
29. Chiarello, G.L., Ferri, D., and Selli, E. (2011). Effect of the CH_3OH/H_2O ratio on the mechanism of the gas-phase photocatalytic reforming of methanol on noble metal-modified TiO_2. J. Catal. ***280***(2): 168–177. https://doi.org/10.1016/j.jcat.2011.03.013.
30. Xie, S., Shen, Z., Deng, J., et al. (2018). Visible light-driven C-H activation and C-C coupling of methanol into ethylene glycol. Nat. Commun. ***9***(1): 1181. https://doi.org/10.1038/s41467-018-03543-y.
31. Chiarello, G.L., Aguirre, M.H., and Selli, E. (2010). Hydrogen production by photocatalytic steam reforming of methanol on noble metal-modified TiO_2. J. Catal. ***273***(2): 182–190. https://doi.org/10.1016/j.jcat.2010.05.012.
32. Shaik, S., Mandal, D., and Ramanan, R. (2016). Oriented electric fields as future smart reagents in chemistry. Nat. Chem. ***8***(12): 1091–1098. https://doi.org/10.1038/nchem.2651.
33. Shaik, S., Danovich, D., Joy, J., et al. (2020). Electric-Field Mediated Chemistry: Uncovering and Exploiting the Potential of (Oriented) Electric Fields to Exert Chemical Catalysis and Reaction Control. J. Am. Chem. Soc. ***142***(29): 12551–12562. https://doi.org/10.1021/jacs.0c05128.
34. Shaik, S., Ramanan, R., Danovich, D., et al. (2018). Structure and reactivity/selectivity control by oriented-external electric fields. Chem. Soc. Rev. ***47***(14): 5125–5145. https://doi.org/10.1039/c8cs00354h.
35. Liu, X.C., Wang, T., Zhang, Z.M., et al. (2022). Reaction Mechanism and Selectivity Tuning of Propene Oxidation at the Electrochemical Interface. J. Am. Chem. Soc. ***144***(45): 20895–20902. https://doi.org/10.1021/jacs.2c09105.
36. Yue, L., Li, J., Zhou, S., et al. (2017). Control of Product Distribution and Mechanism by Ligation and Electric Field in the Thermal Activation of Methane. Angew. Chem. Int. Ed. ***56***(34): 10219–10223. https://doi.org/10.1002/anie.201703485.
37. Joy, J., Stuyver, T., and Shaik, S. (2020). Oriented External Electric Fields and Ionic Additives Elicit Catalysis and Mechanistic Crossover in Oxidative Addition Reactions. J. Am. Chem. Soc. ***142***(8): 3836–3850. https://doi.org/10.1021/jacs.9b11507.
38. Liu, M., Pang, Y., Zhang, B., et al. (2016). Enhanced electrocatalytic CO_2 reduction via field-induced reagent concentration. Nature ***537***(7620): 382–386. https://doi.org/10.1038/nature19060.
39. Wang, C., Li, J., Shao, T., et al. (2023). Electric Field Enhanced Ammoxidation of Aldehydes Using Supported Fe Clusters Under Ambient Oxygen Pressure. Angew. Chem. Int. Ed. ***62***(51): e202313313. https://doi.org/10.1002/anie.202313313.
40. Hill, N.S., and Coote, M.L. (2018). Internal Oriented Electric Fields as a Strategy for Selectively Modifying Photochemical Reactivity. J. Am. Chem. Soc. ***140***(50): 17800–17804. https://doi.org/10.1021/jacs.8b12009.

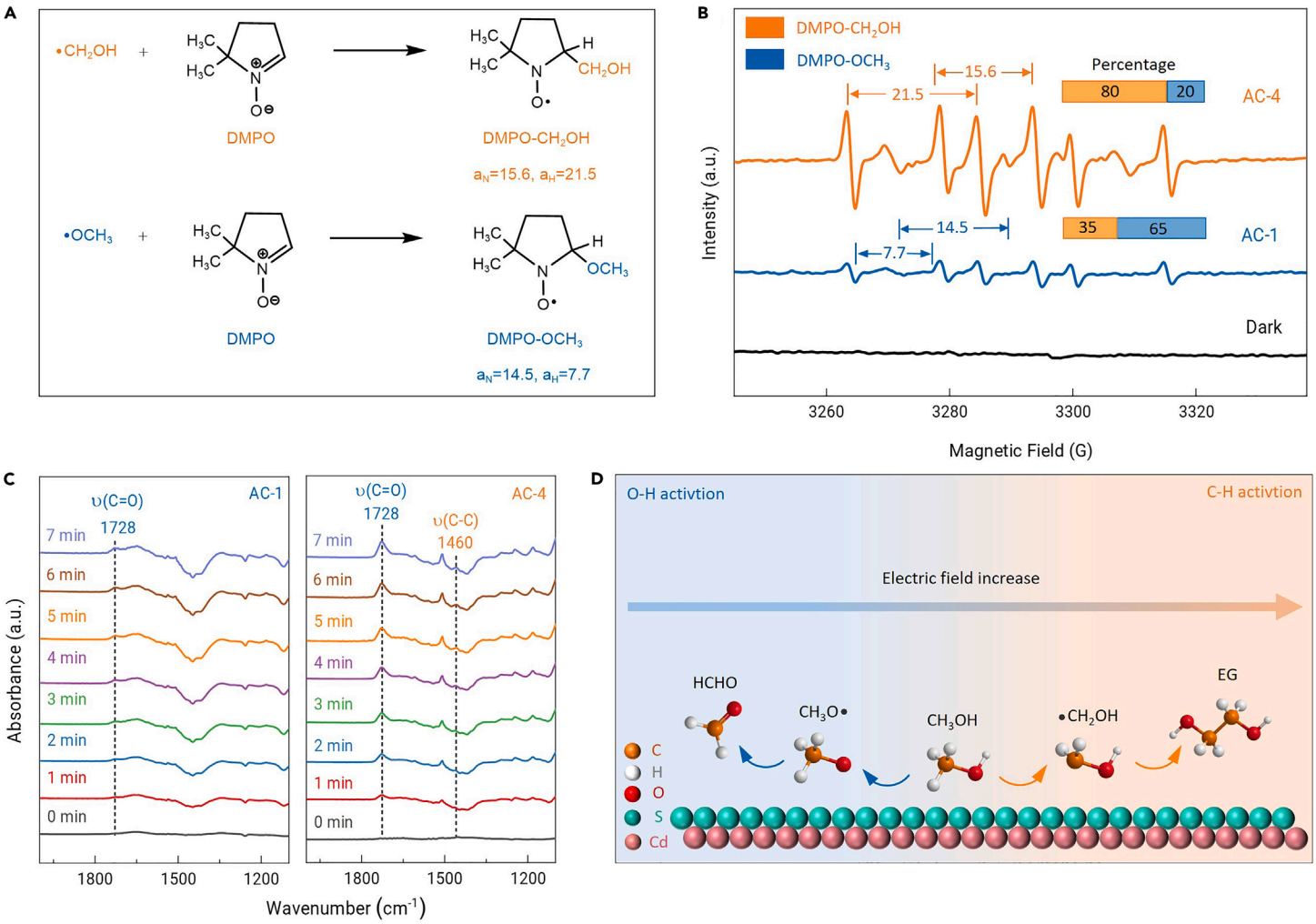

Figure 5. Reaction mechanism in the electric field (A and B) *In situ* electron spin resonance spectra in the presence of 5,5-dimethyl-1-pyrroline-N-oxide (a spin-trapping agent) with or without light irradiation. (C) Time-resolved attenuated total reflection-FTIR spectra of methanol on AC-1 and AC-4 samples. (D) Scheme of electric field on the pathways of methanol conversion.

41. Han, T., Cao, X., Sun, K., et al. (2021). Anion-exchange-mediated internal electric field for boosting photogenerated carrier separation and utilization. Nat. Commun. ***12***(1): 4952. https://doi.org/10.1038/s41467-021-25261-8.
42. Li, J., Cai, L., Shang, J., et al. (2016). Giant Enhancement of Internal Electric Field Boosting Bulk Charge Separation for Photocatalysis. Adv. Mater. ***28***(21): 4059–4064. https://doi.org/10.1002/adma.201600301.
43. Hu, Y., Pan, Y., Wang, Z., et al. (2020). Lattice distortion induced internal electric field in TiO_2 photoelectrode for efficient charge separation and transfer. Nat. Commun. ***11***(1): 2129. https://doi.org/10.1038/s41467-020-15993-4.
44. Ciampi, S., Darwish, N., Aitken, H.M., et al. (2018). Harnessing electrostatic catalysis in single molecule, electrochemical and chemical systems: a rapidly growing experimental tool box. Chem. Soc. Rev. ***47***(14): 5146–5164. https://doi.org/10.1039/c8cs00352a.
45. Stuyver, T., Ramanan, R., Mallick, D., et al. (2020). Oriented (Local) Electric Fields Drive the Millionfold Enhancement of the H-Abstraction Catalysis Observed for Synthetic Metalloenzyme Analogues. Angew. Chem. Int. Ed. ***59***(20): 7915–7920. https://doi.org/10.1002/anie.201916592.
46. Qin, Y., Yu, T., Deng, S., et al. (2022). RuO_2 electronic structure and lattice strain dual engineering for enhanced acidic oxygen evolution reaction performance. Nat. Commun. ***13***(1): 3784. https://doi.org/10.1038/s41467-022-31468-0.
47. Wang, L., Sun, Y., Zhang, F., et al. (2023). Precisely Constructed Metal Sulfides with Localized Single-Atom Rhodium for Photocatalytic C-H Activation and Direct Methanol Coupling to Ethylene Glycol. Adv. Mater. ***35***(5): e2205782. https://doi.org/10.1002/adma.202205782.
48. Gao, Z., Mu, J., Zhang, J., et al. (2022). Hydrogen Bonding Promotes Alcohol C-C Coupling. J. Am. Chem. Soc. ***144***(41): 18986–18994. https://doi.org/10.1021/jacs.2c07410.
49. Shaik, S., Chen, H., and Janardanan, D. (2011). Exchange-enhanced reactivity in bond activation by metal-oxo enzymes and synthetic reagents. Nat. Chem. ***3***(1): 19–27. https://doi.org/10.1038/nchem.943.
50. VanNatta, P.E., Ramirez, D.A., Velarde, A.R., et al. (2020). Exceptionally High O-H Bond Dissociation Free Energy of a Dicopper(II) mu-Hydroxo Complex and Insights into the Geometric and Electronic Structure Origins Thereof. J. Am. Chem. Soc. ***142***(38): 16292–16312. https://doi.org/10.1021/jacs.0c06425.
51. Zhang, Z., Wang, M., Zhou, H., et al. (2021). Surface Sulfate Ion on CdS Catalyst Enhances Syngas Generation from Biopolyols. J. Am. Chem. Soc. ***143***(17): 6533–6541. https://doi.org/10.1021/jacs.1c00830.
52. Dou, Z., Zhang, Z., Zhou, H., et al. (2021). Photocatalytic Upgrading of Lignin Oil to Diesel Precursors and Hydrogen. Angew. Chem. Int. Ed. ***60***(30): 16399–16403. https://doi.org/10.1002/anie.202105692.
53. Li, Z., Huang, W., Liu, J., et al. (2021). Embedding CdS@Au into Ultrathin $Ti_{3-x}C_2T_y$ to Build Dual Schottky Barriers for Photocatalytic H_2 Production. ACS Catal. ***11***(14): 8510–8520. https://doi.org/10.1021/acscatal.1c02018.
54. Cao, Y., Guo, L., Dan, M., et al. (2021). Modulating electron density of vacancy site by single Au atom for effective CO_2 photoreduction. Nat. Commun. ***12***(1): 1675. https://doi.org/10.1038/s41467-021-21925-7.
55. Hu, S., and Li, W.-X. (2021). Sabatier principle of metal-support interaction for design of ultrastable metal nanocatalysts. Science ***374***(6573): 1360–1365. https://doi.org/10.1126/science.abi9828.
56. He, T., Wang, W., Shi, F., et al. (2021). Mastering the surface strain of platinum catalysts for efficient electrocatalysis. Nature ***598***(7879): 76–81. https://doi.org/10.1038/s41586-021-03870-z.
57. Kong, F., Zhou, H., Chen, Z., et al. (2022). Photoelectrocatalytic Reforming of Polyol-based Biomass into CO and H_2 over Nitrogen-doped WO_3 with Built-in Electric Fields. Angew. Chem. Int. Ed. ***61***(42): e202210745. https://doi.org/10.1002/anie.202210745.
58. Kanata-Kito, T., Matsunaga, M., Takakura, H., et al. (1990). Photoreflectance characterization of built-in potential in MBE-produced As-grown GaAs surface. Proc. SPIE ***1286***: 56–65. https://doi.org/10.1117/12.20837.
59. Zhou, H., Wang, M., and Wang, F. (2022). Oxygen-controlled photo-reforming of biopolyols to CO over Z-scheme CdS@g-C_3N_4. Chem ***8***(2): 465–479. https://doi.org/10.1016/j.chempr.2021.10.021.
60. Kumar, R., Sudhaik, A., Raizada, P., et al. (2023). Integrating K and P co-doped g-C_3N_4 with $ZnFe_2O_4$ and graphene oxide for S-scheme-based enhanced adsorption coupled photocatalytic real wastewater treatment. Chemosphere ***337***: 139267. https://doi.org/10.1016/j.chemosphere.2023.139267.

61. Gelderman, K., Lee, L., and Donne, S.W. (2007). Flat-Band Potential of a Semiconductor: Using the Mott–Schottky Equation. J. Chem. Educ. ***84***(4): 685. https://doi.org/10.1021/ed084p685.
62. Zhang, Z., and Yates, J.T., Jr. (2012). Band bending in semiconductors: chemical and physical consequences at surfaces and interfaces. Chem. Rev. ***112***(10): 5520–5551. https://doi.org/10.1021/cr3000626.
63. Stevanovic, A., Büttner, M., Zhang, Z., et al. (2012). Photoluminescence of TiO_2: effect of UV light and adsorbed molecules on surface band structure. J. Am. Chem. Soc. ***134***(1): 324–332. https://doi.org/10.1021/ja2072737.
64. Zhou, H., Wang, M., and Wang, F. (2021). Oxygen-vacancy-mediated catalytic methanation of lignocellulose at temperatures below 200°C. Joule ***5***(11): 3031–3044. https://doi.org/10.1016/j.joule.2021.07.001.
65. Ai, Y., Hu, Z.N., Liang, X., et al. (2021). Recent Advances in Nanozymes: From Matters to Bioapplications. Adv. Funct. Mater. ***32***(14): 2110432. https://doi.org/10.1002/adfm.202110432.
66. Wang, L., Meng, H., Shen, P.K., et al. (2011). In situ FTIR spectroelectrochemical study on the mechanism of ethylene glycol electrocatalytic oxidation at a Pd electrode. Phys. Chem. Chem. Phys. ***13***(7): 2667–2673. https://doi.org/10.1039/c0cp01913e.

ACKNOWLEDGMENTS

This work was supported by the National Natural Science Foundation of China (22372023), the Natural Science Foundation of Liaoning Province (2022-MS-141), and the Research and Innovation Team Project of Dalian University of Technology (DUT2022TB10).

AUTHOR CONTRIBUTIONS

Z.C. conducted most of the experiments of the project and the data analysis; H.Z., F.K., and Z.D. performed the data analysis of photocatalysis; M.W. carried out the DFT calculations; M.W. designed the experiments, supervised the research, and revised the manuscript; and all authors discussed the results.

DECLARATION OF INTERESTS

The authors declare no competing interests.

SUPPLEMENTAL INFORMATION

It can be found online at https://doi.org/10.1016/j.xinn.2024.100659.

LEAD CONTACT WEBSITE

https://www.x-mol.com/groups/wangmin.